


Slowing 80-ns light pulses by four-wave mixing in potassium vapor

D. Arsenović, M. M. Ćurčić,* T. Khalifa, B. Zlatković, Ž. Nikitović, I. S. Radojičić, A. J. Krmpot, and B. M. Jelenković
Institute of Physics Belgrade, University of Belgrade, Pregrevica 118, 11080 Belgrade, Serbia

 (Received 30 June 2018; published 14 August 2018)

We experimentally and theoretically study propagation of 80-ns Gaussian-like probe pulses in hot potassium vapor under conditions of four-wave mixing (FWM). The atomic scheme for FWM is off-resonant, double- Λ atomic scheme, with pump and probe photons, mediated in the K vapor, generating new probe and conjugate photons. We define the subset of FWM parameters, one-photon pump detuning, two-photon pump-probe Raman detuning, vapor density, the pump Rabi frequencies, when slowed pulses exit the vapor are also Gaussian-like. When Gaussian-like pulses exit the cell we are able to compare theoretical and experimental results for fractional delays and broadening for the probe and conjugate. We have obtained fractional delays above 1. Results of the model are compared with the experiment, with and without the model of Doppler averaging, when the atom velocity distribution is divided into different number of groups. We analyze possible causes for pulse broadening and distortion of slowed probe pulses and show that they are the result of quite different behavior of the probe pulse in the FWM vapor. Besides presenting the first results of slowing 80-ns probe pulses, this work is a useful test of the numerical model and values of parameters taken in the model that are not known in experiments.

DOI: [10.1103/PhysRevA.98.023829](https://doi.org/10.1103/PhysRevA.98.023829)

I. INTRODUCTION

Slow light, or reduced pulse group velocity below the speed of light, was demonstrated in different systems [1–10]. There is a strong interest for slow light because of its applications [11], in particular for all-optical signal processing. Optimizations of different slow light systems are based on results for fractional delays and broadenings of initial pulse waveforms.

There are different protocols and different physical systems for generating slow light and ultimately storage of light. A quantum phenomenon that is widely used for slow light is electromagnetically induced transparency (EIT) [12–15]. Narrow EIT resonance is accompanied by steep dispersion, effectively slowing down wave packets propagating through the medium. EIT for slowing and storing light was applied in many physical systems, very often in alkali-metal vapors [16–18].

Four-wave mixing (FWM), characterized by both quantum and strong nonlinear processes, has been used in the last decade for light slowing [19,20] and storage [21–23]. In a typical FWM scheme, in alkali vapor, pump photons and probe photons couple two sublevels of ground states to the same excited state. The second pump photon simultaneously excites the atom, allowing nonlinear conversion of pump photons into probe and conjugate photons. The process is therefore dominated by a strong photon-photon coupling mediated by the nonlinear medium, and photon conversion. Transmission and gain of twin beams strongly depend on detuning around two-photon Raman resonance. Also, the index of refraction varies strongly around the resonance. The FWM gain compensates optical losses, which is an advantage over the EIT as

a physical system, allowing much longer propagation of probe pulses.

In this work we use the off-resonant double- Λ scheme for FWM in K vapor to theoretically and experimentally investigate propagation of 80-ns probe pulses and generation and propagation of conjugate pulses. This atomic scheme was used before to investigate slow light in Rb [19] and Na [20]. However, there is a growing interest in the behavior of transitions on D lines in potassium vapor [24,25], as well as interest in potassium as an active medium for a study of strong nonlinear processes due to its characteristics [26–30]. Parameters of FWM in [26] simultaneously support two propagation regimes of light pulses, slow and fast light. In our work, we are focused on the FWM regime when this system acts as a slowing and amplifying medium, with obtained fractional delays typically larger than 1. In the model we use Maxwell-Bloch (MB) equations to calculate propagations of pump, probe, and conjugate beams through the K cell. FWM parameters in the study are one-photon detunings of the pump beam Δ , two-photon Raman detuning between pump and probe beams δ , pump and probe Rabi frequencies Ω_d and Ω_p , respectively, pump laser power P_d , and potassium vapor density N_c related to cell temperature T_c . Fixed for all measurements and calculations were phase-matching angle and probe Rabi frequency Ω_p related to the probe power P_p .

Potassium is different from other alkali metals. It has the smallest hyperfine splitting (HFS) of the ground state of all alkali metals [24], smaller than the Doppler width. Comparing theoretical and experimental results, qualitatively in terms of pulse waveforms and quantitatively in terms of fractional delays and broadening, we have tested the model and also values of dephasing and decoherence relaxation rates assumed in the calculations. We have discussed results of

*marijac@ipb.ac.rs

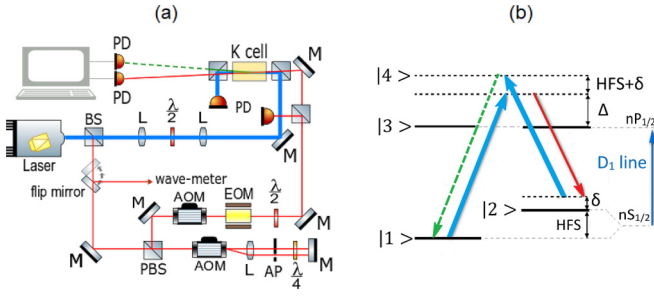


FIG. 1. (a) Experimental setup. (a) Double- Λ scheme for D_1 line in potassium. Pump beam—thick line (blue for online version), probe beam—thin line (red for online version), conjugate beam—dashed line (green for online version).

the model with and without Doppler averaging of density matrix elements. At the end, we have investigated whether there is a relation between the waveform of the outbound slowed probe pulse, which is either broadened Gaussian-like or distorted, and the pulse behavior as it propagates through the K vapor.

II. EXPERIMENT

The schematic of the experiment is shown in Fig. 1. The output from the CW laser (MBR, Coherent) locked to $4S_{1/2}-4P_{1/2}$ D_1 transition in K, at 776 nm, is used for both the pump and the probe beams. A smaller fraction of the probe is sent through two acousto-optic modulators, with the first one in double pass, in order to scan the frequency of the probe beam around Raman resonance with the pump beam frequency. We use the electro-optic modulator to form Gaussian probe pulses. The probe is combined with the pump on the nonpolarizing cube, and both beams are sent to a 4-cm-long vacuum glass cell containing the natural abundance of K vapor. The beams intersect at the center of the cell at the angle of 3 mrad. The pump and the probe beams are linearly and mutually orthogonally polarized with Gaussian radial intensity distribution $1/e^2$ at 1.08 and 0.8 mm, respectively. The K cell was heated by hot air up to 150 °C, or a K density of $1.7 \times 10^{13} \text{ cm}^{-3}$. The probe and the conjugate beams are detected with two photodiodes, and their signals are sent to the storage oscilloscope. Group velocities of the probe and conjugate beams were measured by recording the arrival times of the probe and the conjugate relative to the reference pulse.

The double- Λ scheme was realized on the D_1 line of ^{39}K ($\lambda = 770 \text{ nm}$ [24]), Fig. 1. The pump beam couples the lower hyperfine ground level $4S_{1/2}$, $F = 1$ to the excited $4P_{1/2}$ level with one-photon detuning Δ . Due to the small hyperfine splitting of 55 MHz [24], the hyperfine structure of the $4P_{1/2}$ level is omitted. The probe beam couples the excited $4P_{1/2}$ level to the upper hyperfine ground level $4S_{1/2}$, $F = 2$ and makes a lower Λ scheme with the two-photon Raman detuning δ . Pump photons and new conjugate photons couple $4S_{1/2}$, $F = 2$ to the $4S_{1/2}$, $F = 1$ via an excited state, detuned from the $4P_{1/2}$ levels by $\sim(\Delta + \text{HFS})$, in the upper Λ scheme.

III. THEORETICAL MODEL

Our model describes interaction between ^{39}K atoms in the vapor and electromagnetic (EM) field. The same as in the experiment, four levels of the double- Λ scheme, two ground states $|1\rangle$ and $|2\rangle$, and two excited states $|3\rangle$ and $|4\rangle$, are coupled to produce FWM, Fig. 1. Three components of the total electric field, pump, probe, and conjugate, are denoted by d , p , and c , respectively. The pump couples the $|1\rangle \rightarrow |3\rangle$ and $|2\rangle \rightarrow |4\rangle$ transitions and the probe couples the $|2\rangle \rightarrow |3\rangle$ transition. In the medium, the conjugate beam is generated from optical coherence between levels $|1\rangle$ and $|4\rangle$. Let the energy levels be $E_i = \hbar\omega_i$ with $\omega_3 = \omega_4$, and the angular frequencies of the EM field modes ω_d , ω_p , and ω_c for the pump, probe, and conjugate, respectively. The one-photon detuning is then $\Delta_{(13)} = \omega_d - (\omega_3 - \omega_1)$, and two-photon detuning is $\delta_{(132)} = \omega_d - \omega_p - (\omega_2 - \omega_1)$. Detuning of the conjugate beam is defined as $\Delta_{(1324)} = (2\omega_d - \omega_p) - (\omega_4 - \omega_1)$.

The total electric field

$$\vec{E} = \sum_{i=d,p,c} \vec{e}_i E_i^{(+)} e^{-i\omega_i t + i\vec{k}_i \vec{r}} + \text{c.c.} \quad (1)$$

serves as an interacting potential for ^{39}K atoms. The Hamiltonian is therefore

$$\hat{H} = \hat{H}_0 + \hat{H}_{\text{int}} = \sum_{i=1}^4 \hbar\omega_i |i\rangle\langle i| - \hat{d} \cdot \vec{E}(\vec{r}, t), \quad (2)$$

where \hat{d} is the atomic dipole operator.

To obtain the set of Bloch equations, we first start with the equation for the density matrix

$$\dot{\hat{\rho}} = -\frac{i}{\hbar} [\hat{H}, \hat{\rho}] + \widehat{SE} + \hat{R}, \quad (3)$$

with spontaneous emission \widehat{SE} and relaxation \hat{R} included. We have

$$\widehat{SE} = \sum_{i=1}^4 \Gamma_i (\hat{A}_i \hat{\rho} \hat{A}_i^\dagger - \hat{A}_i^\dagger \hat{A}_i \hat{\rho} / 2 - \hat{\rho} \hat{A}_i^\dagger \hat{A}_i / 2), \quad (4)$$

with $\hat{A}_1 = |1\rangle\langle 3|$, $\hat{A}_2 = |1\rangle\langle 4|$, $\hat{A}_3 = |2\rangle\langle 3|$, $\hat{A}_4 = |2\rangle\langle 4|$, and Γ_i all equal to half of the spontaneous emission rate. The relaxation term is

$$\hat{R} = -\gamma [\hat{\rho} - \text{diag}(\frac{1}{2}, \frac{1}{2}, 0, 0)] - \gamma_{\text{deph}} [\hat{\rho} - \text{diag}(\rho_{11}, \rho_{22}, \rho_{33}, \rho_{44})], \quad (5)$$

where γ and γ_{deph} are relaxation rates. After the substitution,

$$\tilde{\rho}_{ij} = e^{-i\omega_{(ij)}t + i\vec{k}_{(ij)}\vec{r}} \rho_{ij}, \quad (6)$$

where $\omega_{(13)} = \omega_{(24)} = \omega_d$, $\omega_{(23)} = \omega_p$, $\omega_{(14)} = \omega_c$, $\omega_{(12)} = \omega_{(13)} - \omega_{(23)}$, $\omega_{(34)} = \omega_{(14)} - \omega_{(13)}$, $\omega_{(ij)} = -\omega_{(ji)}$, $\vec{k}_{(13)} = \vec{k}_{(24)} = \vec{k}_d$, $\vec{k}_{(23)} = \vec{k}_p$, $\vec{k}_{(14)} = \vec{k}_c$, $\vec{k}_{(12)} = \vec{k}_{(13)} - \vec{k}_{(23)}$, $\vec{k}_{(34)} = \vec{k}_{(14)} - \vec{k}_{(13)}$, $\vec{k}_{(ij)} = -\vec{k}_{(ji)}$, with $\vec{k}_c = 2\vec{k}_d - \vec{k}_p - \Delta\vec{k}$, we apply the rotating wave approximation. The resulting system of differential equations does not have coefficients depending on time. Some coefficients have dependence on $e^{i\Delta k z}$, where $\Delta k = 2k_d(1 - \cos\theta)$, i.e., it is related to the angle θ between the pump and probe beam. Here we set the propagation of the pump in the z direction.

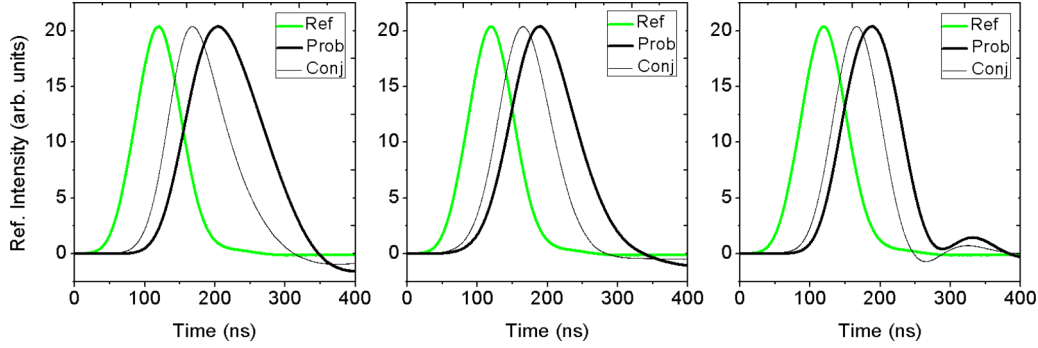


FIG. 2. Experimental observations of slow light, probe (thick black), conjugate (thin black), and reference 80-ns incoming probe beam (green) waveforms for (a) $\delta = -4$ MHz, (b) $\delta = -8$ MHz, and (c) $\delta = -12$ MHz. In all three cases (a), (b), and (c), $\Delta = 0.7$ GHz, $T = 120^\circ\text{C}$, pump power $P_d = 220$ mW, probe power $P_p = 20$ μW .

With a slowly varying envelope approximation, the propagation equations are

$$\left(\frac{\partial}{\partial z} + \frac{1}{c} \frac{\partial}{\partial t}\right) E_d^{(+)} = i \frac{k N_c}{2\epsilon_0} d(\tilde{\rho}_{42} + \tilde{\rho}_{31}), \quad (7a)$$

$$\left(\frac{\partial}{\partial z} + \frac{1}{c} \frac{\partial}{\partial t}\right) E_p^{(+)} = i \frac{k N_c}{2\epsilon_0} d\tilde{\rho}_{32}, \quad (7b)$$

$$\left(\frac{\partial}{\partial z} + \frac{1}{c} \frac{\partial}{\partial t}\right) E_c^{(+)} = i \frac{k N_c}{2\epsilon_0} d\tilde{\rho}_{41}, \quad (7c)$$

where N_c is the atom density.

In order to take into account the Doppler effect, we divide atoms into M groups, each having different z component of the velocity v_z . Due to the Doppler effect these groups differ by effective detuning. Let us denote with $\Delta_{(13)0}$, $\delta_{(132)0}$, and $\Delta_{(1324)0}$ detunings subject to atoms with velocity $v_z = 0$. For an atom with z component of the velocity v_z different than zero, the observed angular frequency ω_o is $\omega_o = \sqrt{\frac{1-\beta}{1+\beta}} \omega_s$, where ω_s is the angular frequency of the light source and $\beta = v_z/c$. The Doppler shift is $\Delta_D = \omega_o - \omega_s$. The detunings are therefore $\Delta_{(13),m} = \Delta_{(13)0} + \Delta_D$, $\delta_{(132),m} = \delta_{(132)0}$, $\Delta_{(1324),m} = \Delta_{(1324)0} + \Delta_D$, where $m = 1, \dots, M$ enumerates velocity groups of atoms. In our model, we keep track of density matrices $\rho_{ij,m}$, $m = 1, \dots, M$ for each group of atoms. There are M sets of Bloch equations. Propagation equations are slightly modified. The source term on the right-hand side of Eq. (8) is the sum of contributions of all groups of atoms:

$$\left(\frac{\partial}{\partial z} + \frac{1}{c} \frac{\partial}{\partial t}\right) E_d^{(+)} = \sum_{m=1}^M i \frac{k N_{c,m}}{2\epsilon_0} d(\tilde{\rho}_{42,m} + \tilde{\rho}_{31,m}), \quad (8a)$$

$$\left(\frac{\partial}{\partial z} + \frac{1}{c} \frac{\partial}{\partial t}\right) E_p^{(+)} = \sum_{m=1}^M i \frac{k N_{c,m}}{2\epsilon_0} d\tilde{\rho}_{32,m}, \quad (8b)$$

$$\left(\frac{\partial}{\partial z} + \frac{1}{c} \frac{\partial}{\partial t}\right) E_c^{(+)} = \sum_{m=1}^M i \frac{k N_{c,m}}{2\epsilon_0} d\tilde{\rho}_{41,m}. \quad (8c)$$

Here $N_{c,m}$ is the atom density of the k th group. We choose $v_{z,m}$ and $N_{c,m}$ to mimic Maxwell distribution $f(v_z) =$

$\sqrt{m/2\pi k_B T} e^{-mv_z^2/2k_B T}$. In the results below, with the Doppler averaging, we have chosen $M = 3$ with Doppler shifts $\Delta_1 = -0.25$ GHz, $\Delta_2 = 0$ GHz, and $\Delta_3 = +0.25$ GHz; the densities are $N_{c,2} = (1.1/3)N_c$ and $N_{c,1} = N_{c,3} = (0.95/3)N_c$.

IV. RESULTS AND DISCUSSION

The probe pulse waveform before the cell is Gaussian with a FWHM of 80 ns; behind the cell the amplified probe and conjugate pulses have different forms. For some FWM parameters they are (broadened) Gaussians, while for others they are distorted. Only when outgoing pulses are Gaussians can we get fractional delays and broadenings. We first present the experimental results, which are compared with the results of numerical simulations, with and without Doppler averaging.

A. Experimental results

We observe propagation of 80-ns probe pulses under conditions of FWM when several parameters are varied. In order to have Gaussian shapes for outgoing probe and conjugate pulses in K vapor, the FWM ought to be realized for densities between $3 \times 10^{12} \text{ cm}^{-3}$ and $\sim 1.75 \times 10^{13} \text{ cm}^{-3}$ (cell temperature 120°C – 150°C), Δ between 700 MHz and 1.3 GHz, and δ in the range ± 10 MHz. Note that not every, or any arbitrary choice of parameter values from the above ranges will produce Gaussian-like pulses at the cell exit. In Fig. 2 we present pulses of reference, probe, and conjugate beams, with their amplitudes normalized to the reference pulse, when $\Delta = 0.7$ GHz for three values of δ , -4 , -8 , and -12 MHz. The resonant probe scatters much more than the conjugate beam, and is slowed more and amplified less than the conjugate, as shown in Fig. 3. The results presented in Fig. 3 are gains, fractional delays, and broadening versus δ obtained from waveforms of Gaussian-like outbound pulses, like the ones shown in Fig. 2. Gains of twin beams are calculated as the ratio of their outbound intensities to the probe inbound intensity. The maximum of probe gain, around 100, is at negative δ , ~ -4 MHz, a small shift from Raman resonance due to Stark shift of energy levels, induced by the blue detuned pump laser. Delays and broadening also have small maximums at these negative values of δ . Maximum values for probe and

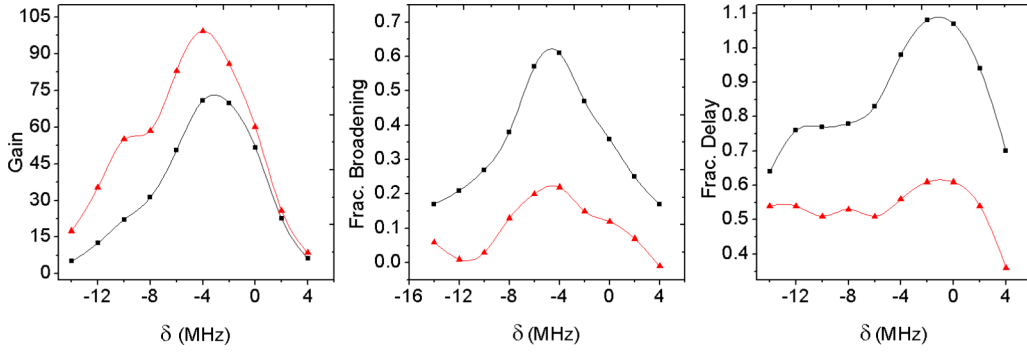


FIG. 3. Probe (solid squares, black for online version) and conjugate (solid triangles, red for online version) (a) gains, (b) fractional broadenings, and (c) fractional delays vs δ , for $\Delta = 0.7$ GHz, $T = 120^\circ\text{C}$, $P_d = 220$ mW, $P_p = 20$ μW .

conjugate fractional delays are ~ 1.08 and ~ 0.6 , while their fractional broadenings are 0.35 and 0.15, respectively.

B. Theoretical results

In the model, the probe entering the cell has a Gaussian profile with 80-ns pulse width and the pump has a constant intensity. The pump and probe detunings, and the gas density correspond to their values in the experiment. However, the model uses parameters whose values are not known in the measurements, such as relaxation coefficients. In the calculations the pump is a plane wave, and although the angle between the pump and the probe is the same as in the experiment, there is a different overlap of two beams in the model than in the experiment. Hence, to find the pump and the probe electric field amplitudes adequate to those in the experiment is not straightforward. We obtain better agreement with measurements if electric field amplitudes in the model are a little lower than those implied by the measurements. The presented results are with Doppler averaging of density matrix elements, assuming three velocity groups for atoms, resulting in three Doppler shifts $\Delta_1 = -0.25$ GHz, $\Delta_2 = 0$ GHz, $\Delta_3 = +0.25$ GHz.

Propagation of EM fields through FWM alkali vapors, when all fields are continuous waves, was discussed in [31]. When probe field is in the form of a pulse, the initial condition for

the MB equations is

$$E_p^{(+)} = E_{p0}^{(+)} \left(f_{dc} + f_{\text{pulse}} e^{-\frac{4 \ln 2 (t - t_{\text{max}})^2}{\text{FWHM}^2}} \right), \quad (9)$$

where FWHM is the pulse full width at half maximum, t_{max} is the time when the pulse reaches peak value, and $f_{dc} + f_{\text{pulse}} = 1$ and represents dc and pulse components. To improve the stability of numerical simulation, we first solve a stationary system where we set $t = 0$ in Eq. (9) and obtain dependencies of z for all unknown variables. These solutions are initial conditions for $t = 0$ in the time propagation of MB equations. Variable parameters in the numerical simulations are the pump and the probe intensities, atom density, θ , Δ , δ , propagation distance z_{max} , and relaxation coefficients. As a result, we have obtained dependencies of the probe and the conjugate beam pulses on t and z . We have found, like in the experiment, that pulse shapes may be Gaussian-like or deformed by a strong asymmetric broadening or presence of multiple peaks.

Similar to the experiment, FWM parameters giving Gaussian-like outgoing pulses in the calculations are limited to a rather small range. Both measurements and the model show more deviations from Gaussian profiles when atom densities are higher or when the gains are lower. In Fig. 4 we present calculated waveforms of the probe and the conjugate pulses at $z_{\text{max}} = 4$ cm.

If outgoing pulses have Gaussian waveforms, we can extract gains and delays of probe and conjugate pulses by fitting the

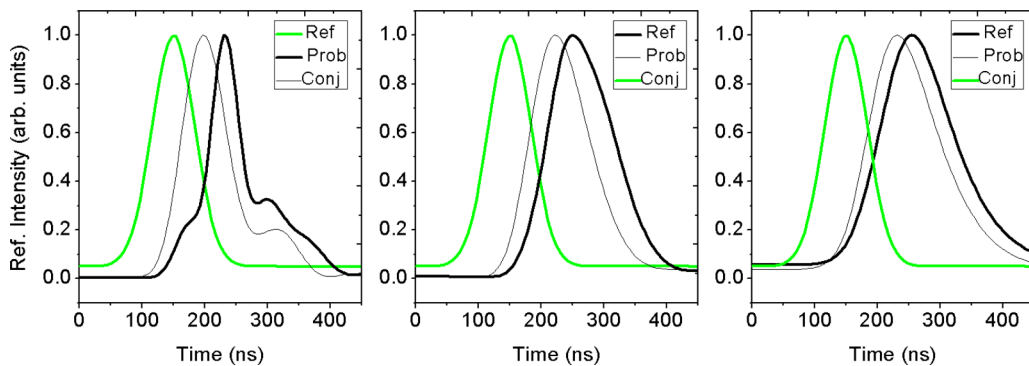


FIG. 4. Calculated waveforms of probe (thick black line) and conjugate (thin black line) for 80-ns incoming probe pulse (green line). (a) $\delta = -4$ MHz, (b) $\delta = -8$ MHz, (c) $\delta = -12$ MHz. Values of other parameters were kept constant, $\Omega_d = 1.38$ GHz, $\Omega_p = 18.9$ MHz, $\gamma = 0.5 \times 10^7$ Hz, $\gamma_{\text{deph}} = 1.5 \times 10^7$ Hz, $\Delta = 0.7$ MHz, $N_c = 3 \times 10^{12}$ cm^{-3} ($T = 120^\circ\text{C}$), $\theta = 3$ mrad.

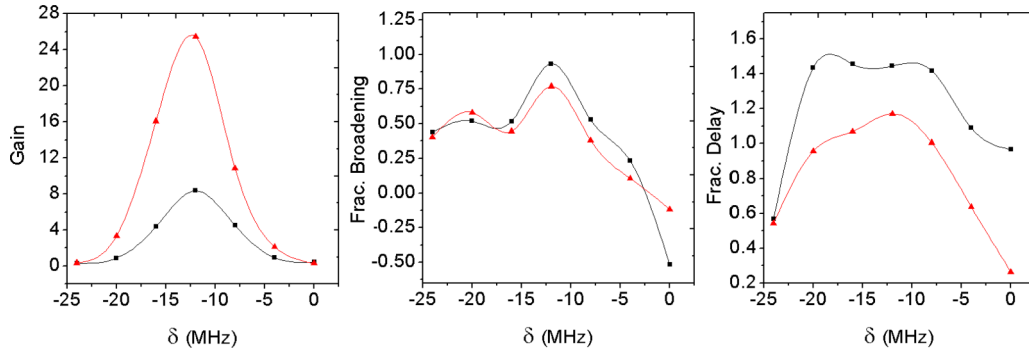


FIG. 5. Calculated probe (solid squares, black for online version) and conjugate (solid triangles, red for online version) (a) gains (note that probe gain is multiplied by 10), (b) fractional broadenings, and (c) fractional delays vs δ of 80-ns input Gaussian pulses in K vapor at $3 \times 10^{12} \text{ cm}^{-3}$ ($T = 120^\circ \text{C}$), $\Omega_d = 1.38 \text{ GHz}$, $\Omega_p = 18.9 \text{ MHz}$, $\Delta = 0.7 \text{ GHz}$.

time dependence of both fields to Gaussian profiles. The fit gives three values, $E_i^{(+)\text{out}}$, $t_{i,\text{maxout}}$, and $FWHM_{i,\text{out}}$, $i = p, c$, for gains, delays, and broadening, respectively. Gains of the probe and the conjugate beams are defined as

$$G_p = \left| \frac{E_p^{(+)\text{out}}}{E_{p0}^{(+)}} \right|^2, \quad (10a)$$

$$G_c = \left| \frac{E_c^{(+)\text{out}}}{E_{c0}^{(+)}} \right|^2. \quad (10b)$$

In Fig. 5 we plot gains, fractional delays, and broadening versus δ for $\Delta = 0.7 \text{ GHz}$ and $N_c = 3 \times 10^{12} \text{ cm}^{-3}$. Gain of the conjugate beam in Fig. 5 is larger than that of the probe, but that is not the general property. At the beginning of the propagation, at $z = 0$, there is only a probe beam, $G_p = 1$ and $G_c = 0$, while at $z = z_{\text{max}}$ we have $G_c > G_p$. Therefore G_p/G_c is directly dependent on z , for other parameters fixed. The values of δ for which gains are maximal depends on the pump intensity, a property known already from the CW regime [31]. Gains have maximums at the negative δ , determined by the detuning Δ and the pump Rabi frequency Ω_d .

In the study of slowing light, we are looking for the range of values of δ where the broadening is low and fractional delay is as high as possible. Similar to the experimental results, this turns out to be the case for $\delta \sim -4 \text{ MHz}$.

Relaxation coefficients are fitting parameters in the model. For $\gamma = 0.5 \times 10^7$ and $\gamma_{\text{deph}} = 1.5 \times 10^7$, we get good agreement with the experiment.

1. Effect of Doppler averaging with different numbers of atom velocity groups

Including the Doppler effect into the model has, for most of the FWM parameters, a strong effect on probe and conjugate waveforms in and behind the vapor. Since Doppler averaging of the density matrix elements can considerably increase computing time, it is also good to know what might be the optimal number of atom velocity groups onto which the velocity distribution is divided. In Fig. 6 we plot the results of the model without taking into account the Doppler effect, top graph (a), with Doppler averaging with three velocity groups, middle graph (b), and with the Doppler averaging using five velocity groups, lower graph (c). Results are for the following parameters: $\Delta = 0.7 \text{ GHz}$ and $\delta = -12 \text{ MHz}$. Values of other parameters in simulations are: $\Omega_d = 3.08 \text{ GHz}$, $\Omega_p = 18.9 \text{ MHz}$, $N = 3 \times 10^{12} \text{ cm}^{-3}$, $\gamma = 5 \times 10^7$, $\gamma_{\text{deph}} = 1.5 \times 10^7$. Having no Doppler averaging gives very much different results than obtained in the experiment. Averaging with three velocity groups gives a more compact profile at the end of the propagating distance. It is broadened with the small secondary peaks, features that measurements have also showed. In the presented case, a further increase of the number of velocity groups does not make a big difference in

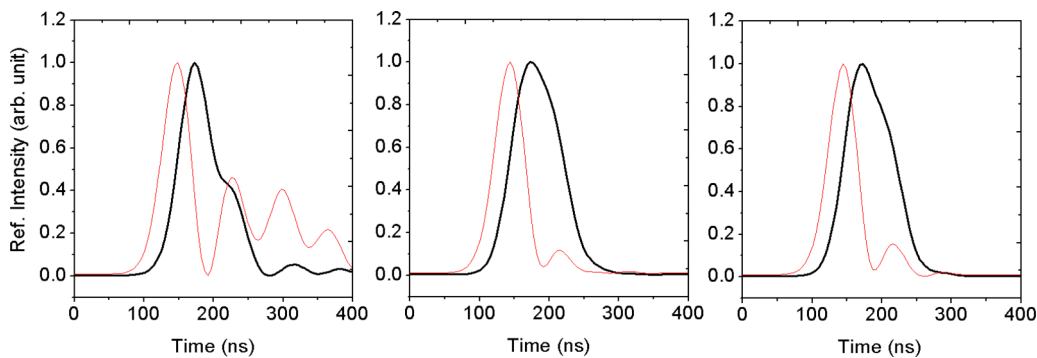


FIG. 6. Numerical simulations of probe (thick black) and conjugate (thin red) waveforms. a) without Doppler averaging, b) with Doppler averaging using 3 velocity groups, and c) using 5 velocity groups. Results are for 80 ns probe inbound pulse, $\Delta = 1 \text{ GHz}$, and $\delta = 4 \text{ MHz}$. Other parameters for simulations: $\Omega_d = 2.31 \text{ GHz}$, $\Omega_p = 18.9 \text{ MHz}$, $N_c = 3 \times 10^{12} \text{ cm}^{-3}$, $\gamma = 5 \times 10^7 \text{ Hz}$, $\gamma_{\text{deph}} = 1.5 \times 10^7 \text{ Hz}$.

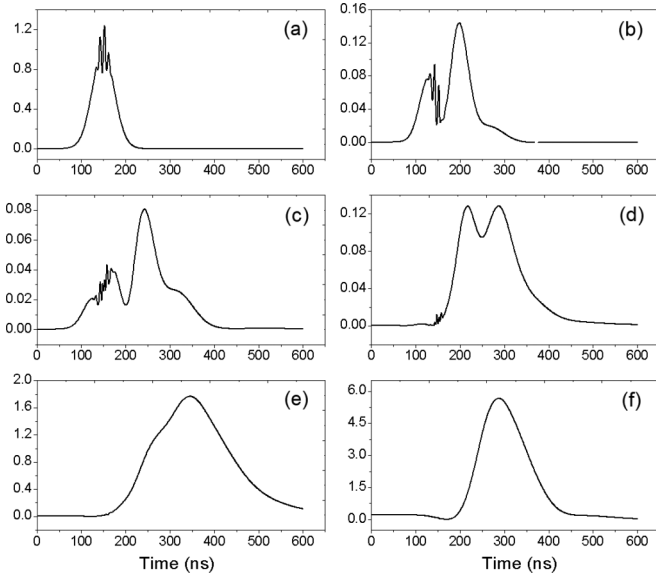


FIG. 7. Dynamics of 80-ns probe pulse propagation through K vapor cell of 4 cm, example of pulse destruction and revival. (a)–(f) Pulse waveforms at 0, 8, 16, 24, 52, and 100% of the total cell length, respectively. Small perturbations at the top of the probe pulse are followed in several figures representing pulse waveform at a later time (distance). Parameters for the simulations: $\Delta = 0.7$ GHz, $\delta = -2$ MHz, $\Omega_d = 3.08$ GHz, $\Omega_p = 18.9$ MHz, $N_c = 3 \times 10^{12}$ cm $^{-3}$, $\gamma = 0.5 \times 10^7$ Hz, $\gamma_{\text{deph}} = 1.5 \times 10^7$ Hz.

the obtained pulse’s waveforms. This is not always the case. For higher pump Rabi frequencies and higher gas temperatures, calculations with five groups of atoms give better agreement with the experiment compared to the ones with three velocity groups. Also, for larger δ , when stronger multiple peaks are observed in the pulse profile, averaging with five velocity groups is a better option. However, one has to be careful with the choice of velocity values.

2. Probe pulse behavior in the hot potassium vapor—Two case studies

Whether the outbound pulse waveform is broadened Gaussian-like or distorted with multiple pulses depends on the pulse behavior from the time it enters the vapor to the time when it exits from the vapor. We have studied probe pulse propagation, while the pulses are at different distances from the (cell) vapor entrance, for two sets of FWM parameters. Both sets of parameters give Gaussian-like outbound pulses, but as we will see below, these pulses exit the vapor after different behaviors while in the vapor. To ease comparison of different and sometimes complex behavioral studies of pulses in the K vapor, we numerically followed propagation of the marker, placed on the top of the probe input pulse, in respect to propagation of the pulse itself. This wavelet is so small that it does not generate an additional effect on the behavior of the pulse, its delay, or broadening. By following the location of the marker versus the pulse peak, we show that the Gaussian pulse at the output may not be directly connected to the input pulse by a time evolution. Instead, another pulses, behind the initial, start to appear, and with enough gain at the end of the

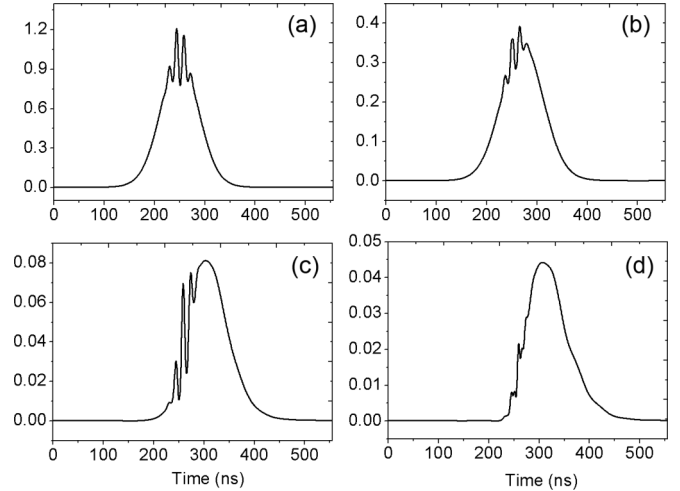


FIG. 8. Dynamics of 80-ns probe pulse propagation through K vapor cell of 4 cm, example of pulse broadening. (a)–(d) Pulse waveforms at different percentages of cell length, 0%, 20%, 60%, 100%, respectively. $\Omega_d = 1.72$ GHz, $N_c = 1 \times 10^{12}$ cm $^{-3}$ ($T = 110$ °C), $\Delta = 0.7$ GHz, and $\delta = 0$ MHz. γ and γ_{deph} are the same as in Fig. 7.

propagation distance, they dominate over the initial pulse. An example is given in Fig. 7 for the following parameters: $\Delta = 0.7$ GHz, $\delta = -2$ MHz, $\Omega_d = 3.08$ GHz, $\Omega_p = 18.9$ MHz, $N_c = 3 \times 10^{12}$ cm $^{-3}$, $\gamma = 0.5 \times 10^7$, $\gamma_{\text{deph}} = 1.5 \times 10^7$. It is clear from the location of the marker that the pulse entering the cell disappears at about $z = 0.6 \times z_{\text{max}}$ (2.5 cm from the entrance). The choice of parameters for results in Fig. 7 give a broadened and slightly distorted outbound pulse, and we see that the secondary pulses, in the high-gain regime, are responsible for the slowed light pulse and broadening.

In Fig. 8 we give an example of pulse propagation when the initial pulse is preserved, i.e., the same pulse travels from the entrance to the exit of the medium. It is only slowed and broadened, and as seen from the graphs in Fig. 8, the marker is slipping behind the pulse peak as it slowed more than the probe pulse. Observed pulse broadening is the result of the pulse front traveling faster than the back of the pulse.

The different behavior of pulses in Figs. 7 and 8 is at different gas density and pump power. This type of simulation shows that for some parameters, there will be only the primary pulse, while for others, secondary pulses may appear, in the vapor and at the exit. The additional pulses may be small, or dominate, or can completely replace the initial pulse, depending on the length of the vapor cell. For ranges of FWM parameters both theory and measurement give complex waveforms of outbound pulses, which theory describes as the result of a generation of new pulses. The secondary pulse is more delayed and less broadened than the primary, and thus offers new possibilities for slow light applications.

V. CONCLUSION

Gains, frictional delays, and broadening of probe and conjugate pulses after 80-ns probe pulses traverses the 4-cm K vapor cell have been measured and calculated when FWM is generated by the double- Λ scheme. Of the broad range of FWM parameters good for parametric gains in the

medium, only the small subrange is good for slowing Gaussian pulses. Both the experiment and the model have shown that an outbound pulse is a nondistorted Gaussian only when every FWM parameter is in a specific, small subrange: $0.7 \text{ GHz} < \Delta < 1.3 \text{ GHz}$, $-16 \text{ MHz} < \delta < 4 \text{ MHz}$, $3 \times 10^{12} \text{ cm}^{-3} < N_c < 9.96 \times 10^{12} \text{ cm}^{-3}$. Both model and experiment have shown that maximum fractional delays are at the maximum of pulse broadening, and typically at two-photon detuning when gains of the probe and conjugate have the highest values. The maximal fractional delays are 1 in the experiment and 1.4 in the model.

We have shown that without Doppler averaging the model fails to reproduce correct pulse profiles. For more complex waveforms, Doppler averaging over a larger number of atom velocity groups, a minimum of 5, might be needed. Following the time (and distance) propagation of the small wavelet, placed at the top of the probe pulse at the cell entrance, in respect to

the propagation of the probe pulse itself, we have shown that, depending on the FWM parameters, the outbound Gaussian-like pulse is the result of quite different pulse propagation dynamics in the vapor. In some cases the initial pulse will disappear and new one can be formed, and for a sufficient gain or length of the vapor, a newly generated pulse will dominate the waveform of the outbound pulse.

ACKNOWLEDGMENTS

The authors acknowledge financial help from Grants No. III45016 and No. OI131038 of the Ministry of Education, Science, and Technological Development of Serbia, MP COST 4103 NQO and IZ73Z0 152511, Joint Research Projects (SCOPEs). We are thankful to M. Minić for thoughtful discussions and help with the electronics.

-
- [1] M. M. Kash, V. A. Sautenkov, A. S. Zibrov, L. Hollberg, G. R. Welch, M. D. Lukin, Y. Rostovtsev, E. S. Fry, and M. O. Scully, *Phys. Rev. Lett.* **82**, 5229 (1999).
 - [2] R. M. Camacho, M. V. Pack, and J. C. Howell, *Phys. Rev. A* **73**, 063812 (2006).
 - [3] R. M. Camacho, M. V. Pack, J. C. Howell, A. Schweinsberg, and R. W. Boyd, *Phys. Rev. Lett.* **98**, 153601 (2007).
 - [4] J. E. Sharping, Y. Okawachi, and A. L. Gaeta, *Opt. Express* **13**, 6092 (2005).
 - [5] Y. Okawachi, M. S. Bigelow, J. E. Sharping, Z. Zhu, A. Schweinsberg, D. J. Gauthier, R. W. Boyd, and A. L. Gaeta, *Phys. Rev. Lett.* **94**, 153902 (2005).
 - [6] A. V. Turukhin, V. S. Sudarshanam, M. S. Shahriar, J. A. Musser, B. S. Ham, and P. R. Hemmer, *Phys. Rev. Lett.* **88**, 023602 (2001).
 - [7] E. Baldit, K. Bencheikh, P. Monnier, J. A. Levenson, and V. Rouget, *Phys. Rev. Lett.* **95**, 143601 (2005).
 - [8] P.-C. Ku, F. Sedgwick, C. J. Chang-Hasnain, P. Palinginis, T. Li, H. Wang, S.-W. Chang, and S.-L. Chuang, *Opt. Lett.* **29**, 2291 (2004).
 - [9] H. Su and S. L. Chuang, *Opt. Lett.* **31**, 271 (2006).
 - [10] M. S. Bigelow, N. N. Lepeshkin, and R. W. Boyd, *Phys. Rev. Lett.* **90**, 113903 (2003).
 - [11] J. B. Khurgin and R. S. Tucker, *Slow Light Science and Applications* (CRC Press, Boca Raton, FL, 2009).
 - [12] A. Kasapi, M. Jain, G. Y. Yin, and S. E. Harris, *Phys. Rev. Lett.* **74**, 2447 (1995).
 - [13] L. V. Hau, S. E. Harris, Z. Dutton, and C. H. Behroozi, *Nature (London)* **397**, 594 (1999).
 - [14] J. Zhang, G. Hernandez, and Y. Zhu, *Opt. Lett.* **31**, 2598 (2006).
 - [15] J. J. Longdell, E. Fraval, M. J. Sellars, and N. B. Manson, *Phys. Rev. Lett.* **95**, 063601 (2005).
 - [16] L. Ma, O. Slattery, P. Kuo, and X. Tang, *Proc. SPIE* **9615**, Quantum Communications and Quantum Imaging XIII **9615**, 96150D (2015).
 - [17] D. Budker, D. F. Kimball, S. M. Rochester, and V. V. Yashchuk, *Phys. Rev. Lett.* **83**, 1767 (1999).
 - [18] D. F. Phillips, A. Fleischhauer, A. Mair, R. L. Walsworth, and M. D. Lukin, *Phys. Rev. Lett.* **86**, 783 (2001).
 - [19] V. Boyer, C. F. McCormick, E. Arimondo, and P. D. Lett, *Phys. Rev. Lett.* **99**, 143601 (2007).
 - [20] J. Okuma, N. Hayashi, A. Fujisawa, and M. Mitsunaga, *Opt. Lett.* **34**, 1654 (2009).
 - [21] Y.-F. Fan, H.-H. Wang, X.-G. Wei, A.-J. Li, Z.-H. Kang, J.-H. Wu, H.-Z. Zhang, H.-L. Xu, and J.-Y. Gao, *Phys. Lett. A* **376**, 785 (2012).
 - [22] R. M. Camacho, P. K. Vudiyasetu, and J. C. Howell, *Nat. Photon.* **3**, 103 (2009).
 - [23] N. B. Phillips, A. V. Gorshkov, and I. Novikova, *Phys. Rev. A* **83**, 063823 (2011).
 - [24] R. K. Hanley, P. D. Gregory, I. G. Hughes, and S. L. Cornish, *J. Phys. B* **48**, 195004 (2015).
 - [25] A. Sargsyan, A. Tonoyan, J. Keaveney, I. G. Hughes, C. S. Adams, and D. Sarkisyan, *J. Exp. Theor. Phys.* **126**, 293 (2018).
 - [26] J. D. Swaim and R. T. Glasser, *Opt. Express* **25**, 24376 (2017).
 - [27] A. Lampis, R. Culver, B. Megyeri, and J. Goldwin, *Opt. Express* **24**, 15494 (2016).
 - [28] B. Zlatković, A. J. Krmpot, N. Šibalić, M. Radonjić, and B. M. Jelenković, *Laser Phys. Lett.* **13**, 015205 (2016).
 - [29] J. D. Swaim and R. T. Glasser, *Phys. Rev. A* **96**, 033818 (2017).
 - [30] M. M. Čurčić, T. Khalifa, B. Zlatković, I. S. Radojičić, A. J. Krmpot, D. Arsenović, B. M. Jelenković, and M. Gharavipour, *Phys. Rev. A* **97**, 063851 (2018).
 - [31] M. T. Turnbull, P. G. Petrov, C. S. Embrey, A. M. Marino, and V. Boyer, *Phys. Rev. A* **88**, 033845 (2013).